Supporting Information

Nanopatterned Titanium Implants Accelerate Bone Formation *In Vivo*

Andrew I. M. Greer[*1]‡, *Vitali Goriainov*[2]‡, *Janos Kanczler*[2], *Cameron RM Black*[2], *Lesley-Anne Turner*[3], *Robert MD Meek*[4], *Karl Burgess*[5], *Ian MacLaren*[6], *Matthew J. Dalby*[3] *and Richard OC Oreffo*[*2], *Nikolaj Gadegaard*[*1]

[1] Division of Biomedical Engineering, School of Engineering, University of Glasgow, G12 8LT, UK

[2] Bone and Joint Research Group, Centre for Human Development Stem Cells and Regeneration, University of Southampton, SO16 6YD, UK.

[3] Centre for Cell Engineering, University of Glasgow, G12 8QQ, UK

[4] Department of Orthopaedics, Queen Elizabeth University Hospital, 1345 Govan Road, Glasgow, Lanarkshire, G51 4TF, UK

[5] Glasgow Polyomics Facility, Institute of Biomedical and Life Sciences, University of Glasgow, G12 8QQ, UK

[6] School of Physics, University of Glasgow, G12 8QQ, UK

‡Both authors contributed equally

* Corresponding authors:

E-mail: Andrew.Greer@glasgow.ac.uk

E-mail: Nikolaj.Gadegaard@glasgow.ac.uk

E-mail: Richard.Oreffo@southampton.ac.uk

Supporting Information

X-ray photoelectron spectroscopy (XPS) analysis

A SAGE 100 system (Specs GmbH, Germany) was used as for the XPS analysis. Base pressure in the analysis chamber was approximately 2e-7 mbar. The X-ray source was MgKα operated at an anode voltage of 12.5 kV and 250 W of power. Spectra were recorded, following a 50 minute Ar sputter, at a take-off angle of 90 degrees. This was carried out to remove the natural oxide formed at the surface as to get more realistic elemental composition of the bulk material. The pass energy for the hemispherical analyser was 50 eV for the survey scans used to determine the elemental composition. Spectra were analysed using casaXPS software, and the elemental composition was determined by integration of peak areas using a standard Shirley background.

XPS was performed on a variety of titania precursor coatings processed with a range of annealing parameters to determine the preferential conditions for removing carbon from the coating. In all cases the furnace was held at maximum temperature for 30 minutes before allowing the furnace to cool down to room temperature overnight.

Following sintering above 500°C, the carbon content (5.5%) of formed TiO_2 was observed to be comparable to the tested commercially pure titanium (cpTi) control (4.5%). Using Raman spectroscopy we found that the polymorph of the formed TiO_2 could be controlled by the annealing temperature (manuscript Figure 1L). Annealing at 300°C produced amorphous TiO_2, 500°C produced anatase whereas 700°C formed rutile. Based on the preponderance in the literature and that both polymorphs have been reported to be biocompatible, the substrates manufactured in this study were annealed to form anatase. This not only ensures biocompatibility for a given biomedical device, but also provides the ability to address specific crystal phases beneficial at the implant surface.

It was discovered that by reducing the annealing rate from 10 °C/minute (as suggested in the literature[1]) to 2°C/minute, the resulting carbon quantity may be significantly reduced from 16% to ~6% for the precursor using 2-methoxyethanol as the diluent. A slight reduction of less than 1 % was recorded when the precursor was adapted by replacing 2-methoxyethanol with 1-hexanol, however this sub – 1 % change is negligible as the detection limit for the XPS machine used is ~1 %. On the same basis an increase in annealing maximum temperature from 500°C to 700°C may also be considered ineffective at reducing the XPS detectable carbon. A control sample of commercially pure titanium (cpTi) was solvent cleaned and subjected to the same XPS analysis as a control to determine the intrinsic level of carbon detectable in cpTi. The result was a carbon level of 4.5%. The results are tabulated in Table S1

Table S1. XPS analysis of sol-gel coated samples where various chemical and annealing parameters have been varied to reduce carbon content. The green box indicates the lowest level detected and the final column contains a control sample of bulk cpTi foil.

Surface:	***Ti***	***Ti***	***Ti***	***Ti***	***Ti***
Coating:	*TiO_2 precursor*	*TiO_2 precursor*	*TiO_2 precursor*	*TiO_2 precursor*	*none*
Precursor solvent:	*2-methoxyethanol*	*2-methoxyethanol*	*1-hexanol*	*1-hexanol*	*N/A*
Anneal maximum temperature:	*500 °C*	*500 °C*	*500 °C*	*700 °C*	*N/A*
Anneal rate:	*10 °C /minute*	*2 °C /minute*	*2 °C /minute*	*2 °C /minute*	*N/A*
Titanium level:	*25.0%*	*28.4%*	*31.0%*	*30.8%*	*25.0%*
Oxygen level:	*58.2%*	*65.3%*	*63.5%*	*62.6%*	*70.5%*
Carbon level:	*16.8 %*	*6.3 %*	*5.5 %*	*6.6 %*	*4.5%*

The conclusion of the XPS analysis is that the preferential annealing conditions for the 1-hexanol based precursor was to anneal with a slow ramp rate of 2°C/minute to a temperature of 500°C (retain the sample at this level for 30 minutes before allowing the furnace to cool overnight) in order to achieve a level of carbon comparable to that present in cpTi.

Water Contact Angle (WCA) analysis

Advancing and receding Sessile drop contact angle measurements were performed on an Attension Theta tensiometer equipped with OneAttension software. An automated syringe pumping system, NanoDrop, was used to deploy 5 µl size drops of RO water onto a variety of relevant substrates in an air atmosphere. Measurements were recorded automatically by the software, and triplicate runs were performed for statistical relevance. The results are displayed in Figure S1.

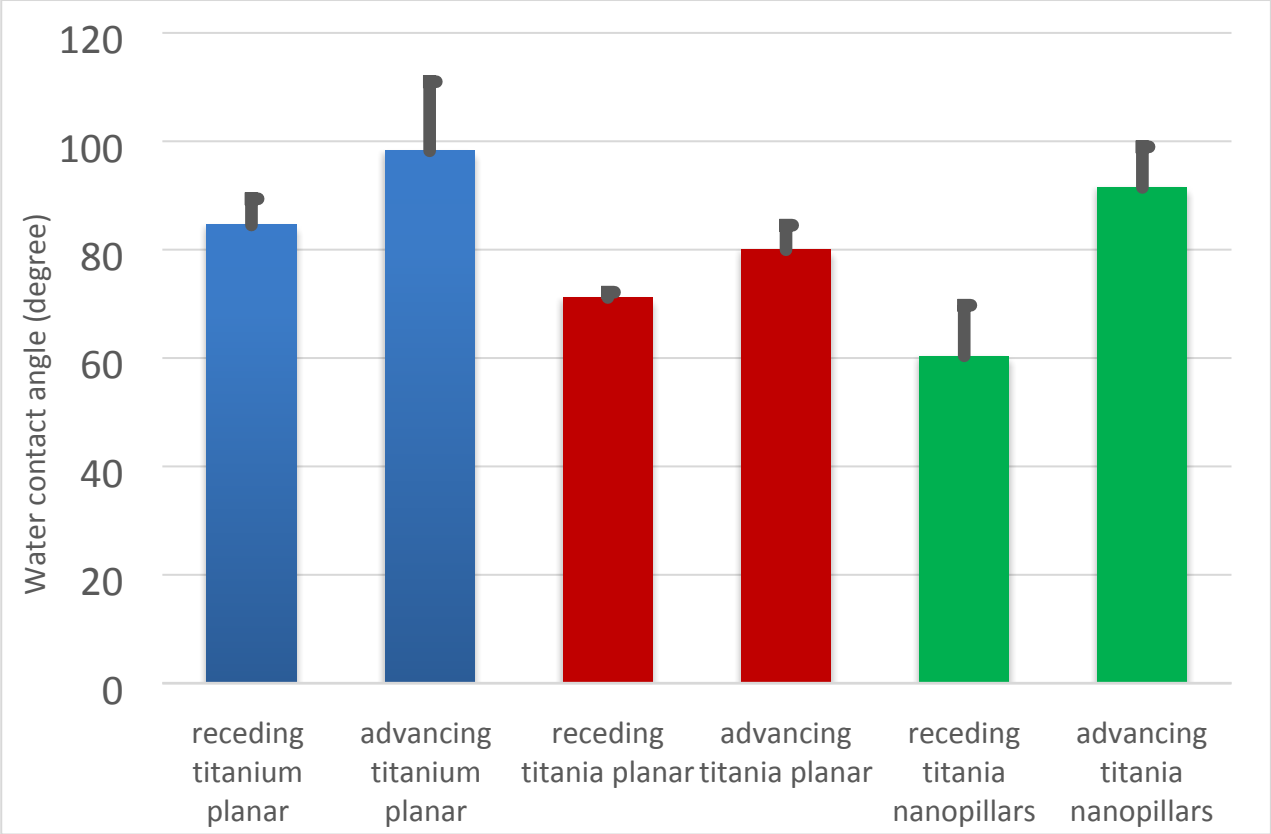

Figure S1. Water contact angles comparison between planar and nanopatterned surfaces. Error bars represent standard deviation from 5 iterations per sample.

Figure S1 indicates that the application of the sol-gel coating was that the water contact angle dropped. Literature has suggested that the formation of titania from a sol-gel precursor will leave hydroxyl (OH) molecules on the surface which explains the reduction in contact angle [2]. The increased hydrophilicity is considered beneficial for bio-integration. One of the most prevalent dental implants was upgraded by the inclusion of packaging which retains the implants hydrophilicity following the surface treatment used in the manufacturers surface roughening process because it has been clinically proven to increase the rate of bone formation [3]. Titania will contain a larger amount of oxygen than naturally oxidised titanium, hence the lower WCA. Given the WCA <90 deg then the nanopillars should further drop the WCA (according to Cassie-Baxter)

which is also visible from the plot. Interestingly, the nanopillars also possess the highest hysteresis which means that the heterogeneity of cells upon the nanopillar surfaces should be better than those without nanopattern.

Raman set-up

Raman point analysis was performed on a Renishaw InVia Raman microscope using a 785 nm wavelength laser. The Renishaw CCD sensor was utilised at 5 exposures per second and 10 traces were accumulated for each spectrum to improve signal-to-noise. The resultant spectra are displayed in the manuscript Figure 1L. The sol-gel coating which was annealed at the lowest tested temperature (300°C) is dominated by noise as the coating is amorphous. The coating annealed at 500°C possesses all of the characteristic peaks of anatase (395,517 and 638 cm^{-1}) and the coating annealed at 700°C shows the expected rutile peaks (447 and 612 cm^{-1}).

TEM & EELS set-up*.* Cross-section slices of the sintered sol-gel coated titanium samples were extracted using focused ion beam milling with a FEI Nova 200 Dual-beam FIB/SEM. STEM and EELS analysis was carried out using a JEOL ARM 200cf operated at 200 kV and equipped with a Gatan GIF Quantum EEL spectrometer.

Establishing optimal nanopillar dimensions for osteogenesis

In order to evaluate the most osteoinductive nanopillar dimensions, a range of heights and diameters of circular disordered nearsquare (NSQ) pillar were fabricated as described in the main text. Each pattern covered a square area of 5x5 mm. The tested nanofeature dimensions are shown in Table S2.

Table S2. Array of tested nanopillar dimensions, 'x' represents a tested dimension.

Diameter (nm) → **Height (nm) ↓**	**40**	**70**	**100**
8	x	x	x
15	x		x
20			x
25	x		
30		x	
40			x
60		x	x
80	x		

The surfaces were each cultured in one well of a six well plate and seeded with 3 ml of bone marrow cells at a concentration of 10,000 cells/ml. Bone marrow contains a large variety of components including STRO1 enriched skeletal stem cells (SSCs), osteoprogenitors and osteoblasts. Thus analysis with this source of cells may not conclude whether the topographies tested upregulate the transformation from an SSC to an osteoblast but it is a very relevant source of cells because in *in vivo* trials individual cell phenotypes will not be found in exclusive populations. The cells were cultured upon the samples for three weeks. At the end of which the samples were fluorescently tagged to identify the cell nucleus (DAPI stain), cell cytoskeleton (actin stain) and bone related proteins osteocalcin (OCN) and osteopontin (OPN) (antibody stain). The production of OCN and OPN are known early indicators of bone formation. By quantifying the amount of OCN and OPN produced per surface one may make a reasonable assumption about the preferential pillar dimensions for bone formation. To analyse the surfaces, a 3 x 3 array of images at 2 mm pitch were captured using a 10x microscope objective which gave a square field of view with side 0.79 mm.

The area of protein visible in each of the nine images per sample was measured with CellProfiler software.[4] The parameters used were thresholds for intensity and size. Primarily the software identified which pixels were within the manually set intensity range – which corresponded to the fluorescent light emitted by the target protein – then disregarded any pixels which were not sufficiently neighbouring with equally bright pixels to satisfy the size thresholds. The number of cells on each sample was also recorded in the same manner using the same software to count the nuclei visible in each image. Dividing the total area of protein on each surface by the total number of nuclei on each surface a value was deduced for the level of protein produced per cell. This value was then made relative to a planar control composed of the same sol-gel derived titania material.

Table S3. Area of OCN protein produced per cell normalised for each nanopillar surface from 9 images (total area = 1447690 pixels) relative to a planar control. Each sample's cell culture batch is represented by the numbers in brackets. The average area of protein produced per control for each batch was b1 = 0.050%, b2 = 0.032%, b3 = 0.032%, b4 = 0.008%.

Diameter (nm) > Height (nm) V	40	70	100
8	0.68 (b1)	0.68 (b2)	0.68 (b3)
15	3.43 (b1)		**7.77 (b4)**
20			3.62 (b4)
25	3.65 (b1), 3.71 (b4)		
30		2.82 (b4)	
40			0.94 (b2)
60		1.17 (b2)	0.32 (b2)
80	1.15 (b4)		

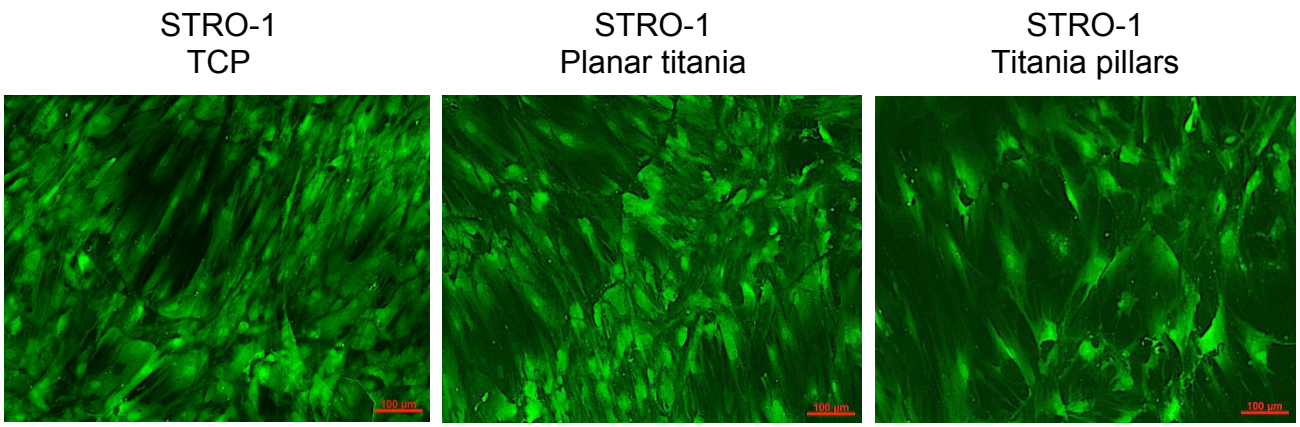

Figure S2. Cell viability assay. Metabolically active cells with intact plasma membrane are stained green with CellTracker Green CMFDA, while damaged or dead cells are stained red with ethidium homodimer-1. CTG/ethidium homodimer-1 co-stain demonstrates viable cells at 21 days of culture on TCP and Titania-coated substrates in basal medium. STRO-1 SSCs on Planar titania surface displayed an elongated and fibroblast-like morphology, in contrast to cells on nanopillars with an enhanced polygonal osteoblast-like morphology. Scale bar 200 µm.

Metabolomics set-up and analysis.

Table S4. All identified metabolites and their corresponding values. Note that metabolites with a confidence score of 9 or 10 match to both retention time (5% window) and accurate mass (3 ppm window) of an authentic standard. Other compounds with scores of 5-8 or lower are matched by reference to a retention time prediction algorithm using the authentic standards as a seed, and should be considered putative assignments.

Metabolite	P value	Fold change	Mass	Retention time	Isomers	Confidence	KEGG ID
N4-(Acetyl-beta-D-glucosaminyl)asparagine	0.05	8.71	335.13	13.07	3	5	C04540
N-Acetylneuraminate	0.06	5.59	309.11	11.77	5	8	C00270
S-Sulfo-L-cysteine	0.03	5.37	200.98	13.86	1	6	C05824
Sulfate	0.07	4.95	97.967	14.02	1	8	C00059
Glu-Met-Phe-His	0.04	4.91	281.11	11.69	1	7	0
Lys-Val-Val	0.04	4.42	172.12	10.92	1	7	0
Guanidinoacetate	0.04	4.06	117.05	13.98	1	8	C00581
2-Hydroxybutane-1_2_4-tricarboxylate	0.04	3.92	206.04	13.8	5	6	C01251
Xanthine	0.05	3.89	152.03	10.68	3	8	C00385
Phosphoenolpyruvate	0.03	3.86	167.98	13.59	3	10	C00074
Picolinamide	0.04	3.77	122.05	7.603	4	5	C01950
N6_N6_N6-Trimethyl-L-lysine	0.09	3.72	188.15	18.69	2	8	C03793
NG_NG-Dimethyl-L-arginine	0.08	3.69	202.14	18.73	3	5	C03626
[FA (20:5)] 5Z_8Z_11Z_14Z_17Z-eicosapentaenoic acid	0.05	3.64	302.22	3.737	43	5	C06428
Oxalate	0.03	3.60	89.995	14.09	1	6	C00209
N-Acetyl-L-histidine	0.04	3.58	197.08	8.276	3	7	C02997
Glyceraldehyde	0.05	3.47	90.032	8.987	6	8	C02154
Lys-Gly	0.07	3.43	203.13	11.54	1	7	0
L-Citrulline	0.04	3.37	175.1	13.74	3	8	C00327
L-Methionine S-oxide	0.08	3.37	165.05	12.02	4	8	C02989
a Cysteine adduct	0.09	3.35	191.03	12.8	1	5	0
D-Glucuronate	0.02	3.34	194.04	13.12	16	6	C00191
Homoarginine	0.04	3.32	188.13	22.77	5	8	C01924
Ethyl 3-oxobutanoate	0.05	3.25	130.06	4.74	17	7	C03500
2_3-Dimethylmaleate	0.06	3.17	144.04	12.63	13	5	C00922
O-Succinyl-L-homoserine	0.02	3.17	219.07	8.798	4	8	C01118
[FA hydroxy_oxo(7:0/2:0)] 4-hydroxy-2-oxo-Heptanedioic acid	0.05	3.16	190.05	10.04	4	6	C05601
L-Valine	0.06	3.13	117.08	11.83	16	10	C00183
ethylpyruvate	0.06	3.12	116.05	4.975	9	7	0
Pyridoxine	0.04	3.06	169.07	8.119	4	10	C00314
2-keto-4-hydroxybutyrate	0.02	3.04	118.03	14.06	7	5	0
Allantoin	0.08	3.01	158.04	12.9	3	8	C01551
N5-Ethyl-L-glutamine	0.06	2.99	174.1	12.29	5	7	C01047
Uracil	0.06	2.97	112.03	8.77	2	10	C00106
(S)-1-Pyrroline-5-carboxylate	0.07	2.95	113.05	12.88	6	6	C03912
L-Tyrosine	0.07	2.94	181.07	12.17	11	10	C00082
L-proline amide	0.07	2.92	114.08	10.99	2	5	0
myo-Inositol	0.01	2.92	180.06	13.04	57	8	C00137
2-Acetolactate	0.02	2.82	132.04	13.05	16	6	C00900
L-Leucine	0.04	2.80	131.09	10.73	12	10	C00123
Ne_Ne dimethyllysine	0.08	2.74	174.14	18.32	1	7	C05545
L-Ornithine	0.09	2.73	132.09	19.01	6	10	C00077
L-1-Pyrroline-3-hydroxy-5-carboxylate	0.02	2.68	129.04	9.637	6	8	C04281
D-Xylulose	0.02	2.67	150.05	13.03	37	6	C00310
D-Galactosamine	0.10	2.66	179.08	12.84	10	8	C02262
L-Histidine	0.01	2.64	155.07	13.11	5	10	C00135
N6-Methyl-L-lysine	0.09	2.63	160.12	19.77	6	6	C02728
L-Serine	0.02	2.62	105.04	13.69	3	10	C00065
2-Hydroxy-2_4-pentadienoate	0.02	2.61	114.03	13.04	6	6	C00596
N(pi)-Methyl-L-histidine	0.09	2.61	169.09	11.82	5	8	C01152
L-Cystine	0.05	2.59	240.02	13.43	2	8	C00491
Methylimidazoleacetic acid	0.04	2.57	v	9.031	7	8	C05828
(S)-1-Pyrroline-5-carboxylate	0.05	2.57	113.05	9.173	6	8	C03912

Hypoxanthine	0.03	2.57	136.04	10.17	3	8	C00262
L-Tryptophan	0.06	2.53	204.09	11.37	6	10	C00078
L-thiazolidine-4-carboxylate	0.02	2.49	133.02	7.647	1	7	0
D-Lysine	0.05	2.46	146.11	20.36	8	8	C00739
Choline	0.07	2.45	103.1	19.79	1	10	C00114
Glu-Phe-Cys-Cys	0.04	2.44	250.07	8.97	1	7	0
HEPES	0.04	2.43	238.1	10.03	1	9	0
Creatinine	0.05	2.41	113.06	9.877	1	10	C00791
cis-Aconitate	0.08	2.35	174.02	13.77	3	8	C00417
L-Phenylalanine	0.04	2.33	165.08	10.22	7	10	C00079
penem CGP31608	0.02	2.33	244.05	10.23	1	5	0
Pantothenate	0.04	2.31	219.11	8.01	1	10	C00864
L-Methionine	0.08	2.24	149.05	11.19	5	10	C00073
Deoxycytidine	0.05	2.17	227.09	10.35	1	6	C00881
Glutarylcarnitine	0.03	2.15	275.14	9.703	1	7	0
Glycine	0.03	2.11	75.032	13.71	3	8	C00037
Pyridoxal	0.04	2.07	167.06	8.136	9	8	C00250
(E)- α-monofluoromethyldehydroarginine	0.07	2.05	102.05	12.78	1	7	0
Asp-Cys-Cys-Ser	0.09	2.03	426.09	13.44	2	5	0
L-Threonine	0.06	2.01	119.06	12.93	11	8	C00188
L-Carnitine	0.09	2.01	161.11	12.23	2	8	C00487
S-Adenosyl-L-methionine	0.09	-2.05	398.14	14.06	1	8	C00019
[FA hydroxy(7:1/2:0)] 2_4-dihydroxy-2-heptenedioc acid	0.03	-2.28	190.05	13.59	4	8	C06201
[PC (14:0/18:2)] 1-tetradecanoyl-2-(9Z_12Z-octadecadienoyl)-sn-glycero-3-phosphocholine	0.04	-3.33	729.53	4.144	14	5	C00157
Tetracosanoic acid	0.01	-3.56	368.37	3.697	5	6	C08320
[PC (14:0/18:1)] 1-tetradecanoyl-2-(11Z-octadecenoyl)-sn-glycero-3-phosphocholine	0.05	-4.90	731.55	4.152	14	5	C00157
[PC (16:0/18:1)] 1-hexadecanoyl-2-(11Z-octadecenoyl)-sn-glycero-3-phosphocholine	0.05	-6.19	759.58	4.212	20	7	C00157
[PG (16:0/18:0)] 1-hexadecanoyl-2-(9Z-octadecenoyl)-sn-glycero-3-phospho-(1'-rac-glycerol) (ammonium salt)	0.02	-7.02	765.55	3.588	1	7	0

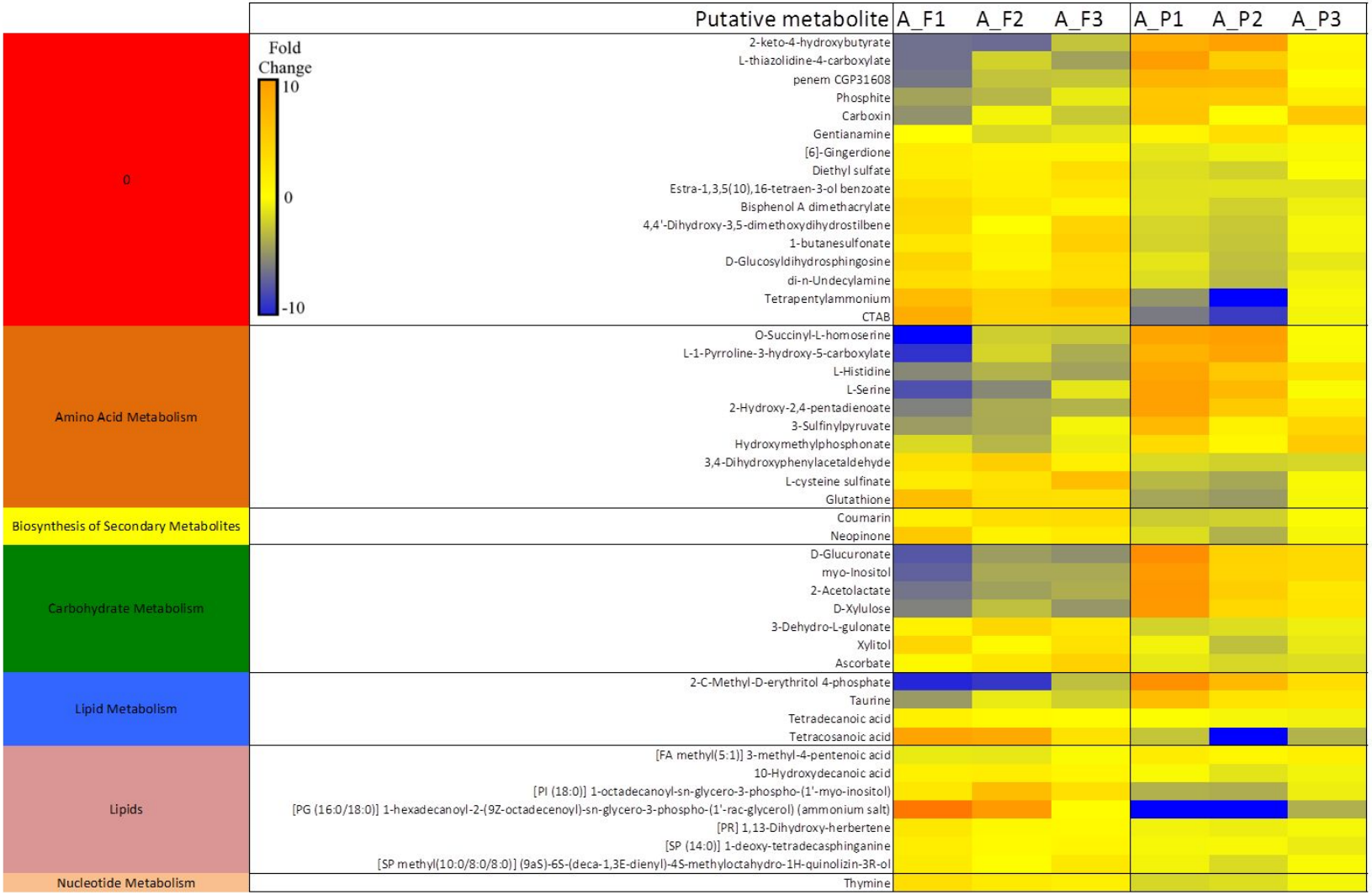

Table S5. Heat map showing fold change per sample for a selection of significantly altered metabolites (t-test with a threshold of P<0.05). Metabolites are putatively assigned based on retention time prediction and accurate mass except where highlighted with an asterix whereby metabolites match to both retention time (5% window) and accurate mass (3 ppm window) of an authentic standard. A_F1 to A_F3 show flat samples 1 to 3; A_P1 to A_P3 show pillar samples 1 to 3.

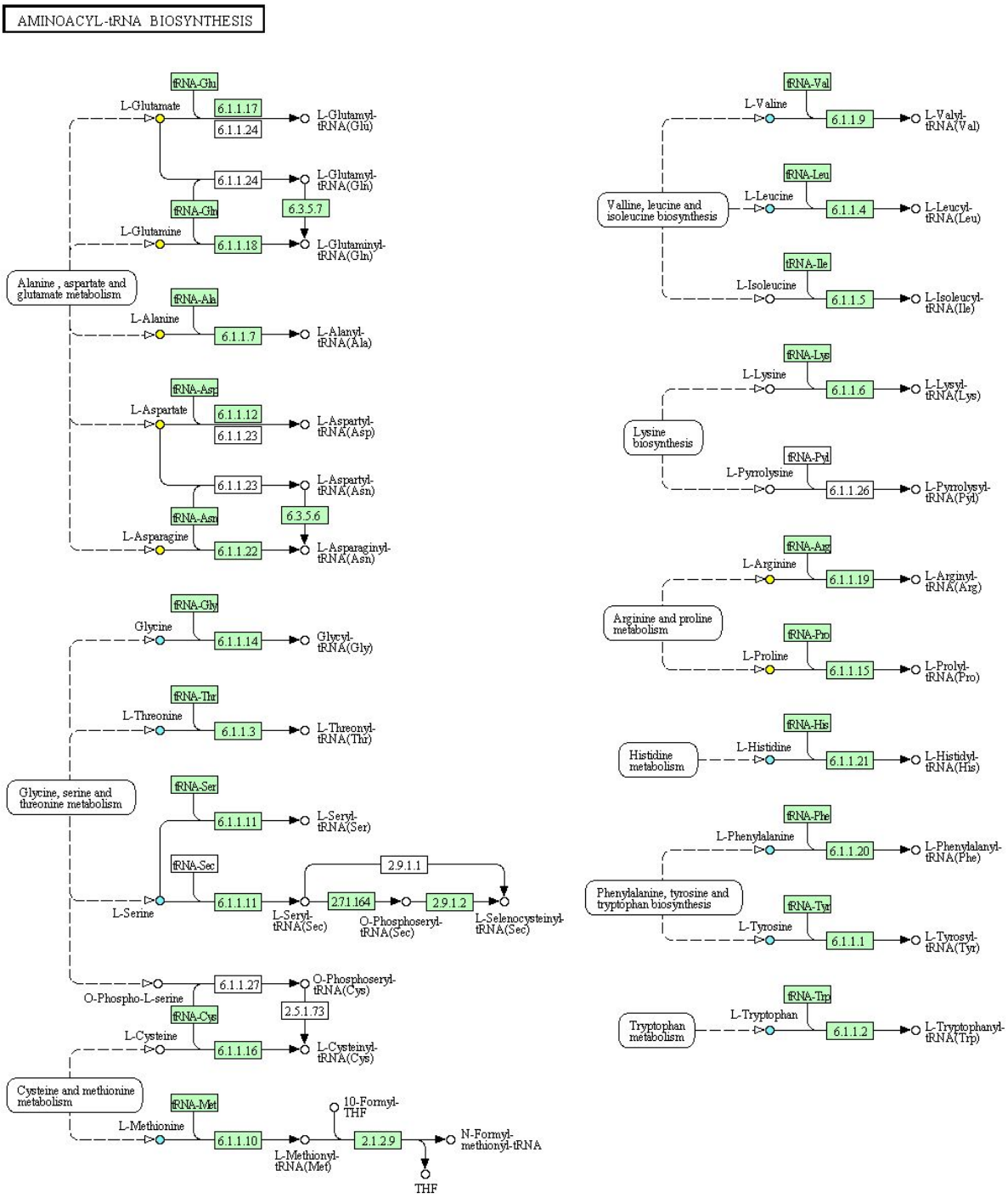

Figure S3. Aminoacyl-tRNA biosynthesis network, highlighting metabolites identified (yellow circles) and showing a greater than 2 fold increase in expression (blue circles) in cells on pillar patterned compared to planar titania substrates. Enzymes are shown in boxes, with enzymes known to be present in humans highlighted in green.

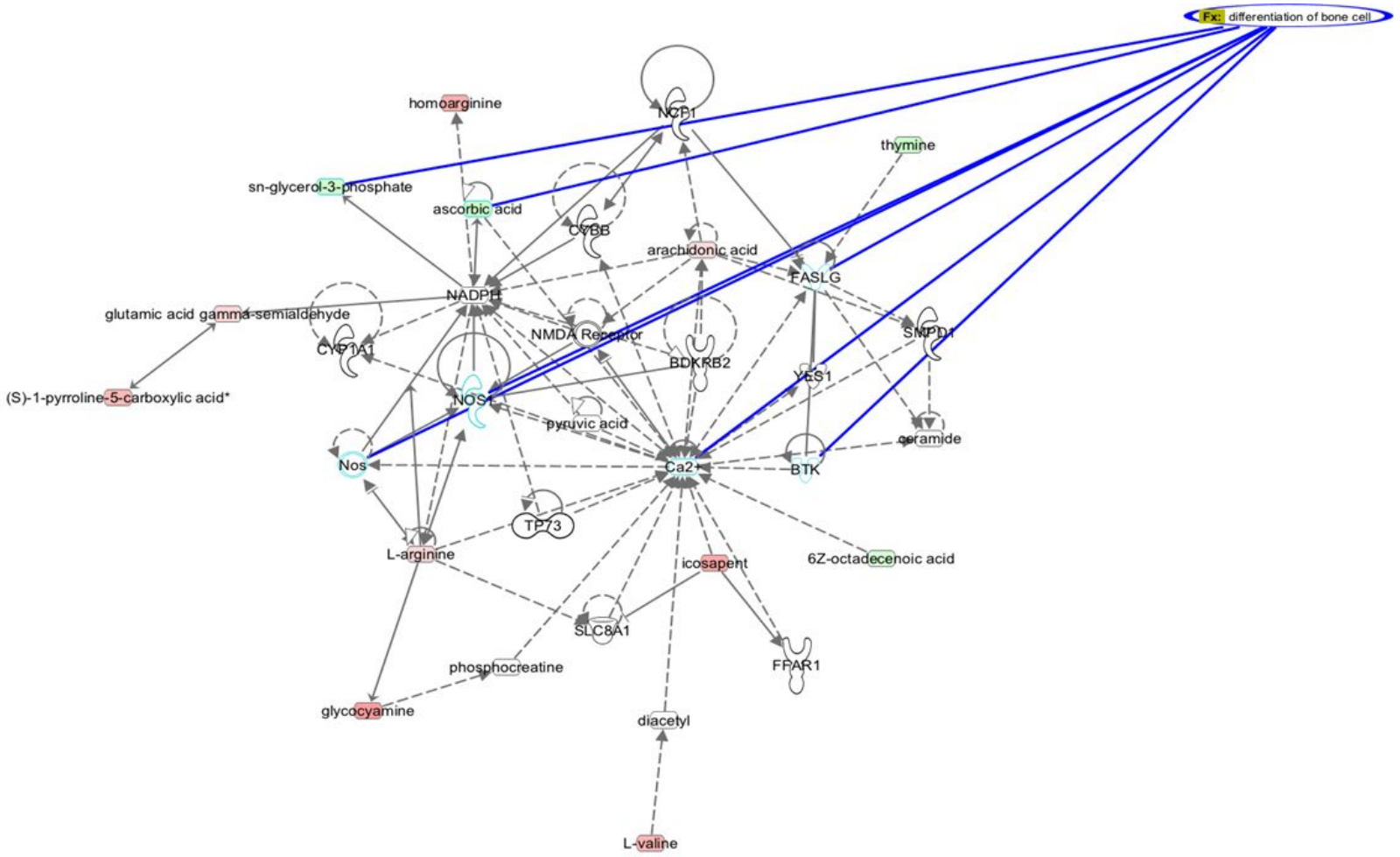

Figure S4. Top ranked biochemical networks altered in osteoprogenitor cells responding to pillar patterned substrates compared to planar. Network highlights bone cell differentiation signalling components such as calcium and ascorbic acid.

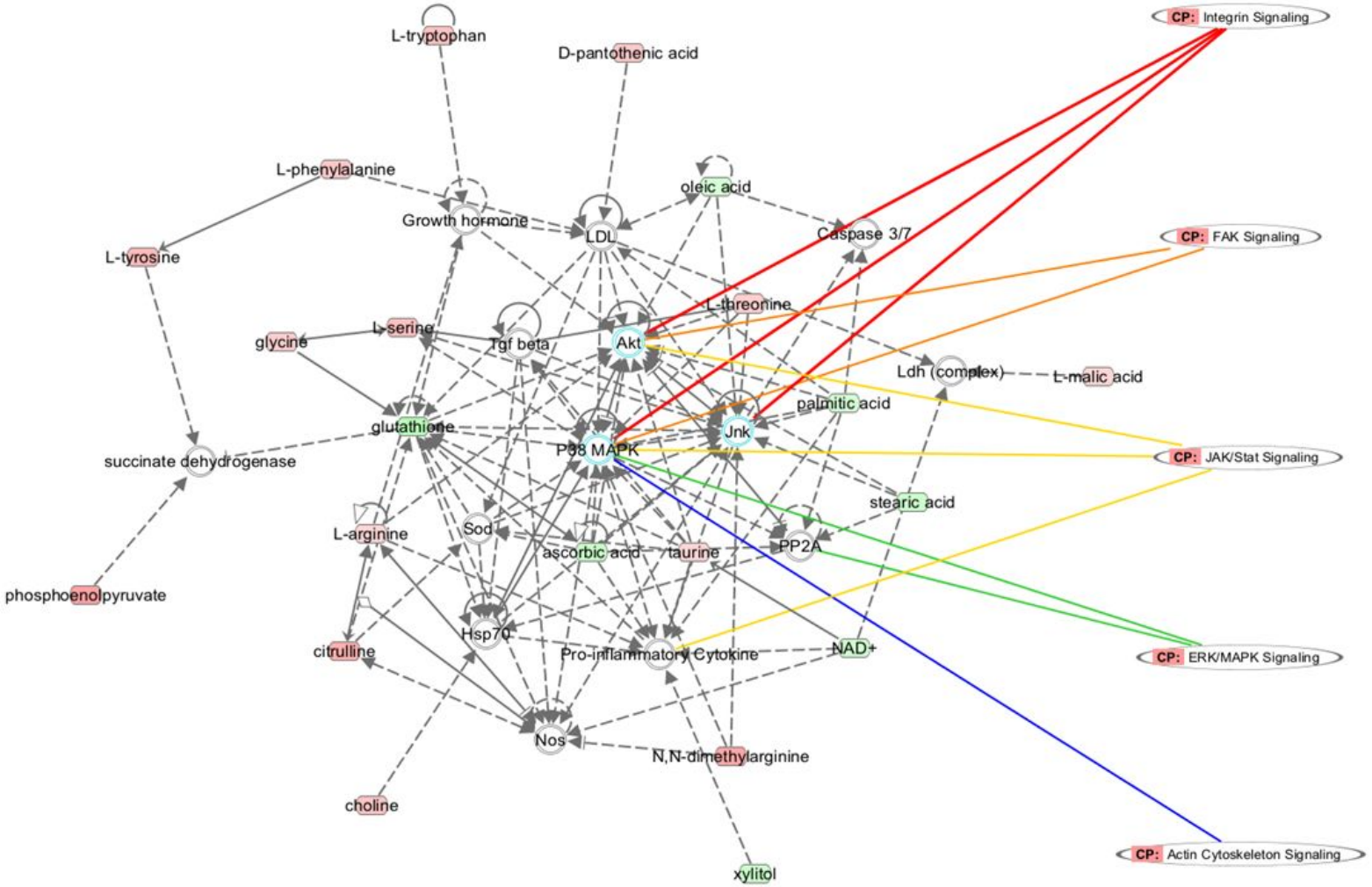

Figure S5. Top ranked biochemical networks altered in osteoprogenitor cells responding to pillar patterned substrates compared to planar. Network highlights mechanotransduction related signalling components such as focal adhesion kinase, integrins and ERK/MAPK signalling.

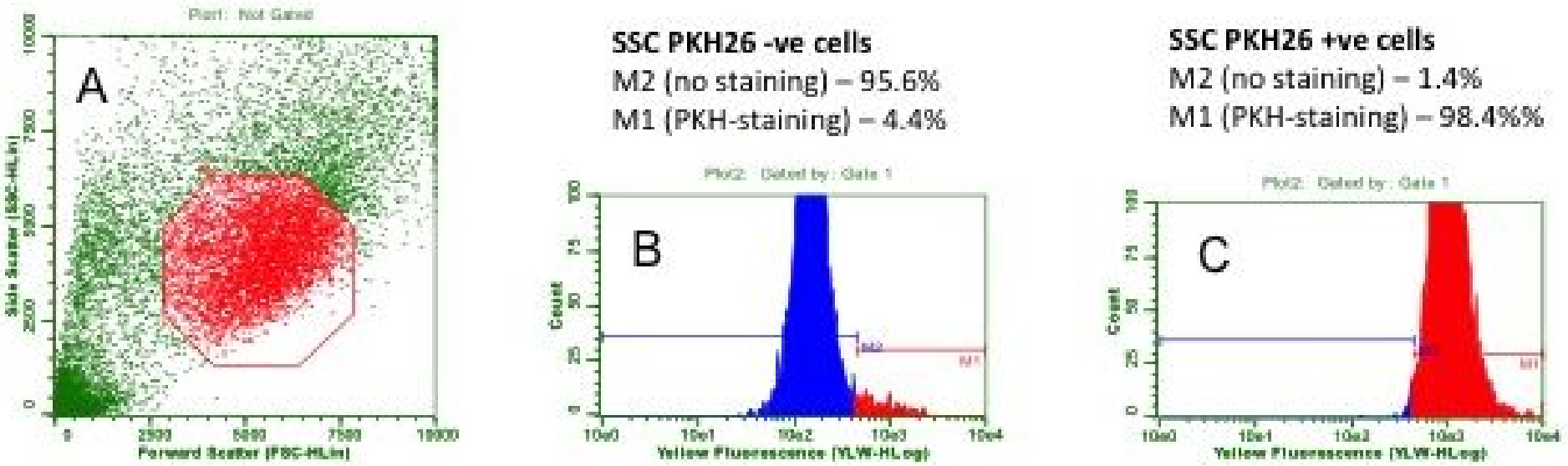

Figure S6. Flow cytometry analysis of PKH26 staining of SSCs prior to seeding. Cells were gated using light forward scattering and side scattering parameters to exclude cell debris/unspecific particles (A). Fluorescence of the gated population was measured using PE-A channel (unstained cells (B), showing significantly lower fluorescence compared to cells stained with PKH26 (C)).

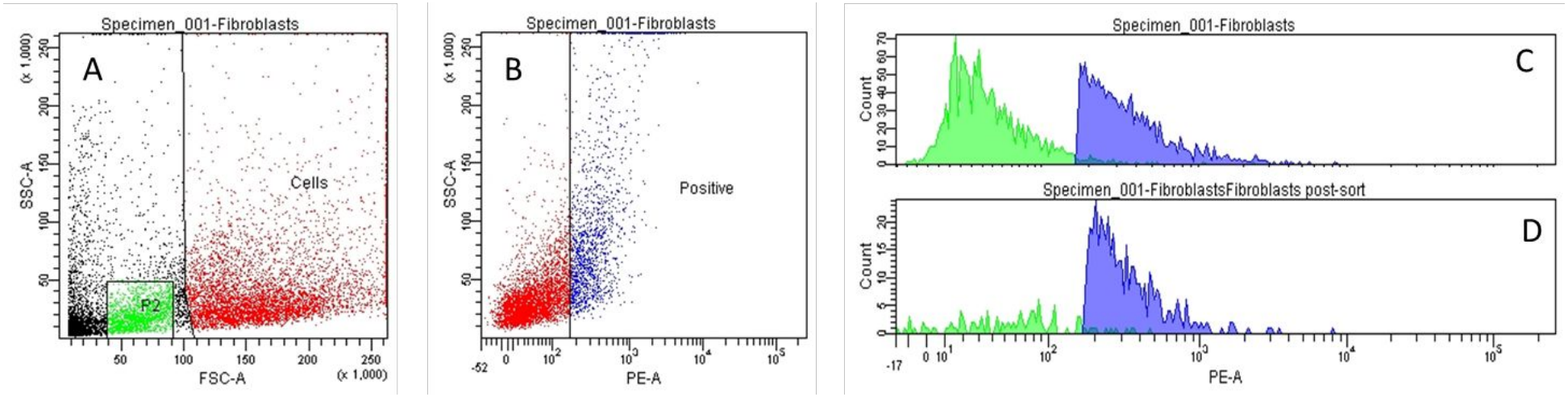

Figure S7. Sample of flow cytometry analysis of cells harvested from the individual substrate groups after 28 days of *in vivo* cultures. Desired cell fraction was identified and selected by light scatter parameters (A) and enriched by selecting fluorescent cells in PE-A channel (B). The cell population isolated (in blue in C), was further examined post initial sort, with relatively high degree of purity revealed in histogram D (high proportion of desired fluorescently labelled cells in blue population).

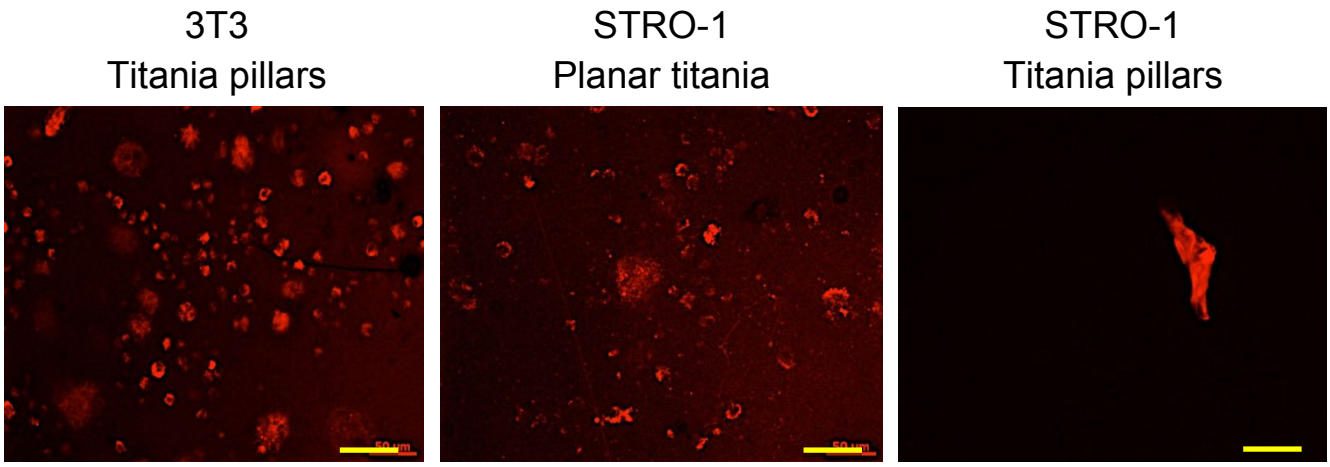

Figure S8. PKH26 fluorescence after substrate retrieval and OPN immunofluorescence of STRO-1 enriched SSCs cultured *in vivo* for 28 days. Scale bar 50 µm.

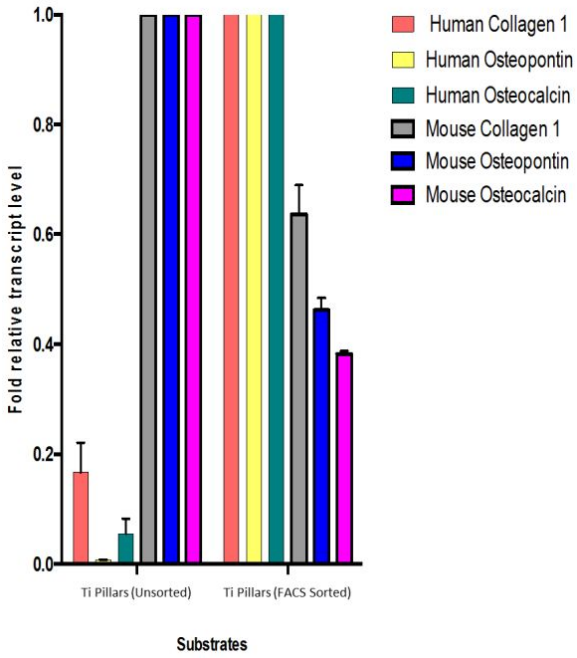

Figure S9. Real-time qPCR analysis of Collagen 1, OPN and OCN gene expression in mouse cells and human STRO-1 enriched SSCs *in vivo* on Titania pillars for 28 days. Comparison between retrieved cell population Unsorted by FACS and FACS Sorted fraction. Human and mouse primers were used and, given Unsorted fraction contained a high proportion of mouse cells, gene expression was normalised against mouse bone marker genes. FACS Sorted fraction was purified by removing the mouse cells to provide a high proportion of fluorescent stained human STRO-1 SSCs and gene expression was normalised against human bone marker genes. (Data expressed as mean ±SD).

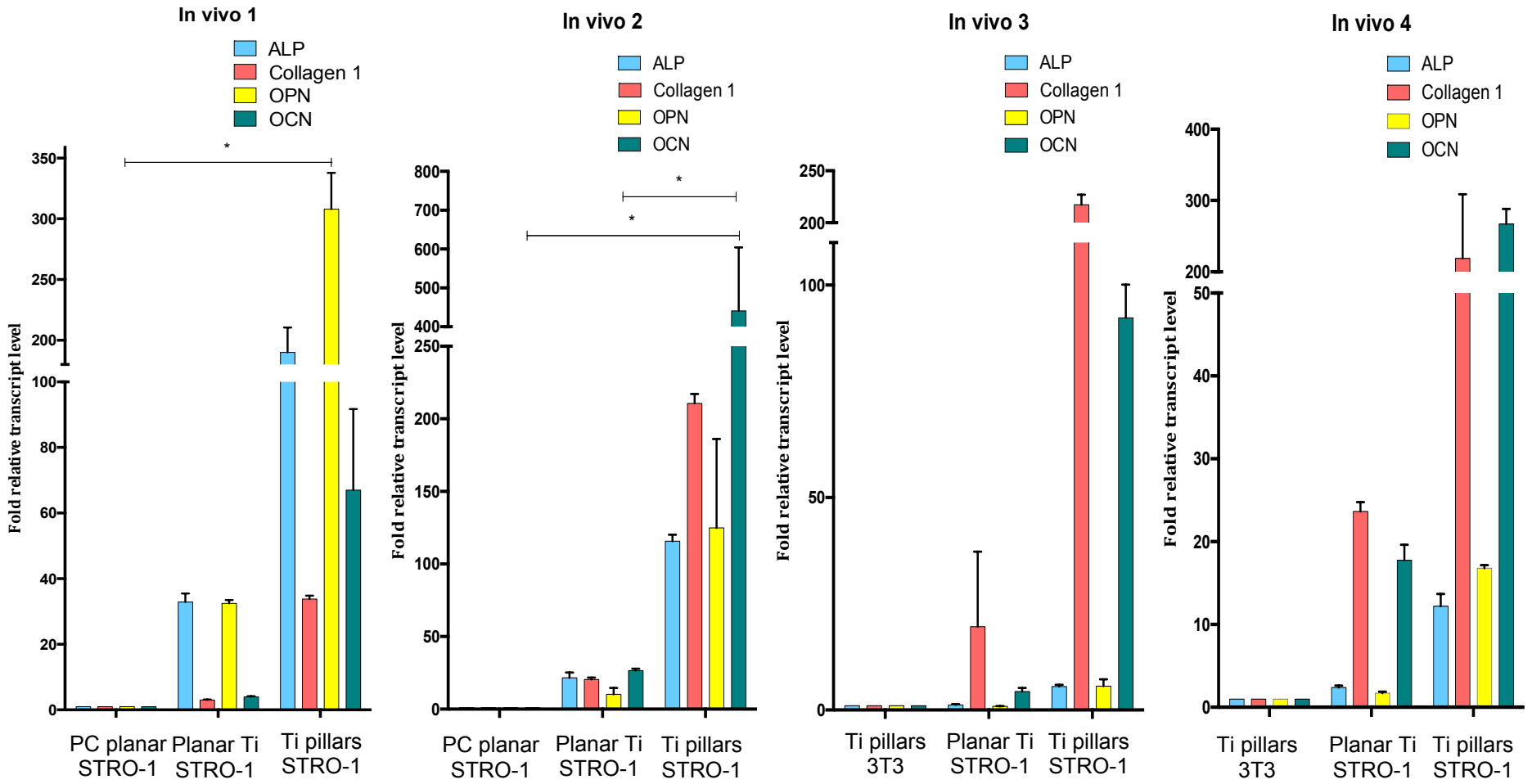

Figure S10. Real-time qPCR analysis of ALP, Collagen 1, OPN and OCN in STRO-1 SSCs cultured *in vivo* on test surfaces and controls for 28 days. STRO-1 PC planar is taken as a negative control in *In vivo 1 and 2*, while 3T3 Ti pillar is taken as a negative control in *In vivo 3 and 4*. Results expressed as mean ± SD, triplicate samples, 2-way ANOVA test, *p<0.05.

Table S6. Primer sequences used for qPCR.				
Species	Gene	Primer pairs	Amplicon	
Human	β-Actin	F: 5' GGC ATC CTC ACC CTG AAG TA 3' R: 5' AGG TGT GGT GCC AGA TTT TC 3'	82	NM_001101
	ALP	F: 5' GGA ACT CCT GAC CCT TGA CC 3' R: 5' TCC TGT TCA GCT CGT ACT GC 3'	86	NM_000478
	Collagen Ia]	F: 5' GAG TGC TGT CCC GTC TGC 3' R: 5' TTT CTT GGT CGG TGG GTG 3'	52	NM_000088
	OPN	F: 5' GTT TCG CAG ACC TGA CAT CC 3' R: 5' CAT TCA ACT CCT CGC TTT CC 3'	80	NM_001251830
	OCN	F: 5' GGC AGC GAG GTA GTG AAG AG 3' R: 5' CTC ACA CAC CTC CCT CCT 3'	102	NM_001199662
Mouse	β-Actin	F: 5' TTG CTG ACA GGA TGC AGA AG 3' R: 5' GTA CTT GCG CTC AGG AGG AG 3'	86	NM_007393
	Collagen Ia]	F: 5' GCC AAG AAG ACA TCC CTG AAG 3' R: 5' TGT GGC AGA TAC AGA TCA AGC 3'	102	NM_007742
	OPN	F: 5' GCT TGG CTT ATG GAC TGA GG 3' R: 5' GGT CCT CAT CTG TGG CAT C 3'	81	NM_001204203
	OCN	F: 5' CTG ACC TCA CAG ATG CCA AG 3' R: 5' ACC TTA TTG CCC TCC TGC TT 3'	76	NM_001037939

Substrate preparation. The substrates were sterilised for a minimum of 24 hrs in PBS/1% antibiotic-antimycotic solution, Life Technologies, then transferred into culture plates and washed in PBS prior to cell seeding.

Live/dead cell assay. Cell viability assay was performed using CellTracker™ Green (CTG) CMFDA and ethidium homodimer-1 (Life Technologies). 50 μg of CTG and 5 μg of ethidium homodimer were dissolved in 10 μl of DMSO, and added to the culture medium.

Fluorescence microscopy. To analyse the surfaces, a 3 x 3 array of images at 3 mm pitch were captured using a 10x microscope objective which gave a square field of view with side 0.79 mm. The area of protein visible in each of the nine images per sample was measured with CellProfiler software. The software parameters used were thresholds for intensity and size. The number of cells upon each sample was also recorded in the same manner using the same software to count the nuclei visible in each image. By dividing the total area of protein on each surface by the total number of nuclei on each surface a value was deduced for the level of protein produced per cell.

Immunofluorescence of OPN ex vivo. Samples were fixed in 4% PFA, blocked with goat serum, Sigma-Aldrich, followed by overnight treatment in anti-OPN primary antibody raised in rabbit (GeneTex) followed by goat anti-rabbit IgG (H+L) secondary antibody, Alexa Fluor® 488 conjugate (Life Technologies). Cells were

counterstained with DAPI (4',6-Diamidino-2-Phenylindole, Dihydrochloride) (Life Technologies), and mounted on slides prior to imaging. Image capture was performed with Zeiss Axiovert 200 inverted microscope using an Axiovert HR camera for white light imaging and Axiocam MR camera for fluorescent imaging. Zeiss Axiovision software version 4.7 was used for image capture and analysis. Confocal imaging was performed with Leica TCS SP5 laser scanning confocal microscope on a Leica DMI6000 inverted microscope stand using LAS-AF software.

qPCR Analysis. Primer sequences are shown in Table S5 with β-actin serving as the house-keeping gene. Primer sequences were validated by dissociation curve/melt curve analysis and efficiencies of amplification for the β-actin primers and primers for the bone marker genes of interest were approximately equal. The comparative cycle threshold method was utilised for quantification of PCR amplification data and relative transcript levels expressed as mean ± S.D. Data were analysed and plotted using GraphPad Prism 6 for Mac OS X software.

References

1. Richmond, D. A.; Zhang, Q.; Cao, G.; Weiss, D. N., Pressureless nanoimprinting of anatase TiO2 precursor films. *J Vac Sci Technol B: Microelectron Nanometer Struct* **2011,** *29* (2), 021603-021603-5.
2. Advincula, M. C.; Rahemtulla, F. G.; Advincula, R. C.; Ada, E. T.; Lemons, J. E.; Bellis, S. L., Osteoblast adhesion and matrix mineralization on sol–gel-derived titanium oxide. *Biomaterials* **2006,** *27* (10), 2201-2212.
3. Oates, T. W.; Valderrama, P.; Bischof, M.; Nedir, R.; Jones, A.; Simpson, J.; Toutenburg, H.; Cochran, D. L., Enhanced implant stability with a chemically modified SLA surface: a randomized pilot study. *Int J Oral Maxillofac Implants* **2007,** *22* (5), 755.
4. Carpenter, A. E.; Jones, T. R.; Lamprecht, M. R.; Clarke, C.; Kang, I. H.; Friman, O.; Guertin, D. A.; Chang, J. H.; Lindquist, R. A.; Moffat, J., CellProfiler: image analysis software for identifying and quantifying cell phenotypes. *Genome biol* **2006,** *7* (10), R100.